

HOW TO FIND A CODIMENSION-ONE HETEROCLINIC CYCLE BETWEEN TWO PERIODIC ORBITS

WENJUN ZHANG, BERND KRAUSKOPF AND VIVIEN KIRK

Department of Mathematics, The University of Auckland,
Private Bag 92019, Auckland 1142, New Zealand

Abstract

Global bifurcations involving saddle periodic orbits have recently been recognized as being involved in various new types of organizing centers for complicated dynamics. The main emphasis has been on heteroclinic connections between saddle equilibria and saddle periodic orbits, called EtoP orbits for short, which can be found in vector fields in \mathbb{R}^3 . Thanks to the development of dedicated numerical techniques, EtoP orbits have been found in a number of three-dimensional model vector fields arising in applications.

We are concerned here with the case of heteroclinic connections between two saddle periodic orbits, called PtoP orbits for short. A homoclinic orbit from a periodic orbit to itself is an example of a PtoP connection, but is generically structurally stable in a phase space of any dimension. The issue that we address here is that, until now, no example of a concrete vector field with a non-structurally stable PtoP connection was known. We present an example of a PtoP heteroclinic cycle of codimension one between two different saddle periodic orbits in a four-dimensional vector field model of intracellular calcium dynamics. We first show that this model is a good candidate system for the existence of such a PtoP cycle and then demonstrate how a PtoP cycle can be detected and continued in system parameters using a numerical setup that is based on Lin's method.

1 Introduction

In numerous fields of application one finds mathematical models with continuous time that take the general form of a vector field

$$\dot{x} = f(x, \lambda), \tag{1}$$

where

$$f : \mathbb{R}^n \times \mathbb{R}^m \rightarrow \mathbb{R}^n$$

is sufficiently smooth, say, twice differentiable for the purpose of this paper. Here \mathbb{R}^n is the phase space of (1) and $\lambda \in \mathbb{R}^m$ is a multi-dimensional parameter. The flow of (1) is denoted by ϕ^t .

To understand the dynamics of (1) one needs to study how the phase space is organised by invariant objects, including equilibria and periodic orbits, and, when the equilibria or periodic orbits are of saddle type, their global stable and unstable manifolds. Furthermore, one needs to study bifurcations, where these objects change qualitatively when the parameter λ is varied. A bifurcation is said to be of codimension d if it is encountered generically at isolated points in a d -dimensional parameter space. A distinction is made between local and global bifurcations: a local bifurcation occurs when there is a change of stability of an equilibrium or a periodic orbit, while a global bifurcation is characterised by the rearrangement of global stable and unstable manifolds. Of particular interest are homoclinic and heteroclinic bifurcations, where one finds a homoclinic or heteroclinic orbit (or connection) that arises as a non-generic intersection of stable and unstable manifolds of a saddle object or of two different saddle objects. It is well known that homoclinic and heteroclinic bifurcations may give rise to complicated behavior, including chaotic dynamics; see, for example, the textbooks [31, 43, 47] for general information about bifurcation theory.

Due to their inherently global nature, the identification of homoclinic or heteroclinic orbits in a given system typically requires the use of advanced numerical methods [4, 5, 12, 13, 18, 22, 29, 23, 24, 42, 48]. A common feature of many of these methods is that the connecting orbit in question is represented by an orbit segment (over a finite time interval) that is the solution of a boundary value problem (BVP) with suitable boundary conditions near equilibria and/or periodic orbits. Homoclinic and heteroclinic orbits to equilibria can be computed readily in this way with, for example, the HOMCONT [12] part of the well-known continuation package AUTO [21]. This makes it possible to perform comprehensive studies of systems with complicated bifurcation diagrams featuring numerous curves of global bifurcations of equilibria; some recent examples can be found in [10, 41].

More recently, heteroclinic cycles in generic vector fields (without additional symmetry properties) involving periodic orbits have attracted considerable interest. The basic examples are the EtoP cycle between a saddle equilibrium and a saddle periodic orbit and the PtoP cycle between two different periodic orbits. When these cycles are of codimension one, they give rise to nearby complicated recurrent dynamics; see, for example, [11, 36, 37, 38, 49, 50, 51]. Most of the emphasis has been on the case of a codimension-one EtoP heteroclinic cycle, which can be found in three-dimensional vector fields. A well-known example is the EtoP heteroclinic cycle in the Lorenz system (where it is responsible for the birth of chaotic dynamics) [25, 42], but EtoP cycles have also been found in a number of vector fields arising in different applications, including models of a food chain [6, 7], of intracellular calcium dynamics [10], of electronic circuits [28], of nonlinear laser dynamics [53], and of a global return mechanism near a saddle-node Hopf bifurcation [40, 42]. The case of PtoP cycles, on the other hand, is much less studied. In fact, as far as we know, all published examples of PtoP connections in concrete vector fields [18, 19, 24, 42] are structurally stable and, hence, of codimension zero. Providing an example of a

vector field with a PtoP connection of codimension $d \geq 1$ is the challenge that is addressed here; we do this with the use of advanced numerical tools.

A number of numerical methods have been developed for the computation of EtoP and PtoP connections. The work of Beyn [5] introduced the general setup and error bounds with projection boundary conditions for such computations. Pampel [48] implemented this scheme to compute a codimension-one EtoP connection in the Lorenz system. This EtoP connection and a codimension-zero PtoP connection in a coupled oscillator system were computed by Dieci and Rebaza [18, 19] by using the continuation of invariant subspaces from [13] to define the boundary conditions. Doedel *et al.* [23] define projection boundary conditions via the adjoint variational equation along a periodic orbit, and continue codimension-one EtoP connections in the Lorenz system and in three-dimensional models of an electronic circuit and of a food-chain; in [24] these authors also compute a codimension-zero PtoP homoclinic orbit of the food-chain model. All these numerical methods represent the EtoP or PtoP connecting orbit as *a single orbit segment*, and they have the common difficulty of finding an initial approximate connecting orbit that satisfies the defining BVP. Pampel [48] finds this start data by continuing intersection curves of (un)stable manifolds in a suitably chosen plane, while Dieci and Rebaza [18, 19] use a simple shooting method. Doedel *et al.* [23, 24], on the other hand, find an initial connecting orbit with a homotopy-type approach (as is used in HOMCONT [12] for connecting orbits between equilibria), which works quite well when the (un)stable manifold of the equilibrium is of dimension one and the phase space is not too large ($n = 3$ in their examples).

In contrast to the above methods, Krauskopf and Rieß [42] represent an EtoP orbit of codimension d in any phase space dimension by *two separate orbit segments*. Their numerical setup is an implementation of Lin’s method [45], which is a theoretical tool for the analysis of recurrent dynamics, in particular near homoclinic orbits and heteroclinic cycles; see, for example, [36, 49, 51, 52, 54]. More specifically, one orbit segment starts near the equilibrium and ends in a suitably chosen section Σ , and the second orbit segment starts in Σ and ends near the periodic orbit. Projection boundary conditions are used near the saddle objects; the conditions are well established near equilibria [4] and adapted from [26] near periodic orbits. The crucial point is that the difference of the end points of the two orbit segments can be restricted to lie in a fixed d -dimensional subspace Z , which is also referred to as the Lin space. After choosing a basis for Z one obtains d well-defined test functions, called the Lin gaps, that measure the (signed) gap sizes along each of the basis vectors. An EtoP orbit can be found by continuation runs that close the Lin gaps one by one, and the EtoP orbit can then be continued in system parameters with the Lin gaps remaining closed. While two orbit segments (rather than just one) need to be computed, the major advantage of the Lin’s method approach is that the overall BVP for the two orbit segments is well posed irrespective of how close the system is to an actual EtoP orbit. As a result, finding start data is not really an issue. Furthermore, other common zeros of the Lin gaps and, hence, more than just one EtoP

connection may be detected with the same setup. The method was demonstrated in [42] with the detection and continuation of codimension-one EtoP connections in the Lorenz system and in the model vector field from [40]; moreover, a codimension-two EtoP connection was computed in a four-dimensional Duffing-type system.

In this paper we use the Lin’s method approach from [42] to find and continue a codimension-one PtoP heteroclinic cycle between two saddle periodic orbits. A brief discussion of how this approach could be adapted for the computation of PtoP connections was already given in [42], but in that paper the method was demonstrated only with the computation of a PtoP heteroclinic connection of codimension zero. The main issue, which we address here, is the lack of an example of a concrete vector field that features a PtoP connection of codimension $d \geq 1$, where the codimension is only due to the dimensions of the (un)stable manifolds and the resulting dimension of a generic intersection. It is not at all straightforward to find such an example. First of all, note that a PtoP homoclinic orbit of a hyperbolic saddle periodic orbit Γ is of codimension $d = 0$ in a phase space of any dimension n , because $\dim(W^u(\Gamma)) + \dim(W^s(\Gamma)) = n + 1$ regardless of the value of n . Hence, one needs to consider PtoP heteroclinic connections between two saddle periodic orbits, Γ_1 and Γ_2 . For a codimension-one PtoP connection to exist, the phase space must be at least four dimensional; in the case that the phase space is \mathbb{R}^4 we must have $k := \dim(W^u(\Gamma_1)) = 2$ and $l := \dim(W^s(\Gamma_2)) = 2$. Where should one look for two periodic orbits with this property? If one can find suitable periodic orbits in a concrete vector field, how can one check that a PtoP connection actually exists?

It is quite clear that, even with numerical continuation tools such as AUTO [21] or MATCONT [16], these questions cannot be answered by an unguided search for saddle periodic orbits in model vector fields with phase spaces of dimension (at least) four. Rather, our approach is to:

- I. provide theoretical insight into a minimal example of a codimension-one PtoP heteroclinic connection and describe the type of bifurcation structure near which one may expect to find such a connection;
- II. implement the Lin’s method approach from [42] for the detection and continuation of PtoP heteroclinic connections;
- III. identify a candidate vector field from a suitable area of application that has the correct ingredients in terms of its bifurcation structure; and
- IV. verify the existence of a codimension-one PtoP heteroclinic connection in the candidate vector field.

In this way, we are able to show that a codimension-one PtoP heteroclinic cycle exists in a four-dimensional model of intracellular calcium dynamics [55]. We are also able to continue the locus of the PtoP cycle as a curve in a parameter plane, and to detect and continue nearby PtoP homoclinic orbits and periodic orbits. In other words, the dynamics near the codimension-one PtoP heteroclinic cycle can now be studied

with advanced numerical tools. We remark in this context that PtoP heteroclinic cycles are closely related to heterodimensional cycles between saddle fixed points of a diffeomorphism. This type of global bifurcation provides a mechanism for generating partially hyperbolic attractors and related complicated dynamics; see, for example, [8, 9, 17] and further references therein, as well as [2, 39].

The structure of the paper is as follows. In Sec. 2 we provide the formal definition of a PtoP orbit of codimension d and then discuss in Sec. 2.1 the specific example of a PtoP heteroclinic cycle in \mathbb{R}^4 . The Lin's method setup for PtoP orbits is introduced in Sec. 3 and its implementation is presented in Sec. 3.1. In Sec. 4 we introduce the four-dimensional simplified Atri model for intracellular calcium dynamics. A partial bifurcation analysis in Sec. 4.2 demonstrates that this model has the geometric elements required for the existence of a codimension-one PtoP heteroclinic cycle. Sec. 5 is devoted to finding and continuing the heteroclinic cycle with the Lin's method approach. The codimension-one PtoP connection is computed in Sec. 5.1 and the codimension-zero PtoP connection is found in Sec. 5.2; the codimension-one PtoP cycle is then continued in Sec. 5.3 as a curve in two system parameters. Sec. 6 shows how PtoP homoclinic orbits and saddle periodic orbits can be found numerically near the codimension-one PtoP cycle. We summarize our findings in Sec. 7.

2 PtoP connection of codimension d

We consider here a heteroclinic connecting orbit Q of (1) between two hyperbolic saddle periodic orbits Γ_1 and Γ_2 that exists for a given value of the parameter $\lambda = \lambda^*$. To be specific, we assume that the connection is such that the flow on it is from Γ_1 to Γ_2 ; if necessary, this can be achieved by reversing time in (1). Hence, we consider the unstable manifold

$$W^u(\Gamma_1) := \{x \in \mathbb{R}^n \mid \lim_{t \rightarrow -\infty} \text{dist}(\phi^t(x), \Gamma_1) = 0\}$$

and the stable manifold

$$W^s(\Gamma_2) := \{x \in \mathbb{R}^n \mid \lim_{t \rightarrow \infty} \text{dist}(\phi^t(x), \Gamma_2) = 0\},$$

which are assumed to intersect in Q , that is, $Q \in W^u(\Gamma_1) \cap W^s(\Gamma_2) \subset \mathbb{R}^n$. We further assume that the following genericity conditions are satisfied.

- (C1) The periodic orbit Γ_1 is hyperbolic and its unstable manifold $W^u(\Gamma_1)$ is of dimension $k \geq 2$.
- (C2) The periodic orbit Γ_2 is hyperbolic and its stable manifold $W^s(\Gamma_2)$ is of dimension $l \geq 2$.

(C3) $k + l \leq n$.

(C4) The connecting orbit Q at $\lambda = \lambda^*$ is isolated and $\dim(T_q W^u(\Gamma_1) \cap T_q W^s(\Gamma_2)) = 1$ for any point $q \in Q$.

(C5) The λ -dependent families of $W^u(\Gamma_1)$ and $W^s(\Gamma_2)$ intersect transversely in the product \mathbb{R}^{n+m} of phase space and parameter space.

Conditions (C1)–(C5) ensure that the only source of codimension of the PtoP connection is due to the dimensions of the two global manifolds $W^u(\Gamma_1)$ and $W^s(\Gamma_2)$, so that $Q \in W^u(\Gamma_1) \cap W^s(\Gamma_2) \subset \mathbb{R}^n$ has the codimension $d := n + 1 - k - l$. Note that $d \geq 1$ due to (C3); hence, the PtoP connection Q can be found along an $(m - d)$ -dimensional subspace of the m -dimensional parameter region Λ . In particular, one encounters the PtoP connection Q generically for $m \geq d$. In the case that (C3) is not satisfied, (that is, for $k + l > n$) the PtoP connection Q is structurally stable (since the intersection of $W^u(\Gamma_1)$ and $W^s(\Gamma_2)$ in \mathbb{R}^n is structurally stable) and we say that Q is of codimension zero. Note further that in this case the connection Q need not be isolated and, hence, condition (C4) may be violated.

2.1 Codimension-one PtoP connection in \mathbb{R}^4

Codimension-one EtoP orbits can occur in \mathbb{R}^3 when the equilibrium has a one-dimensional unstable manifold; a well-known example can be found in the Lorenz system [1, 23, 25, 42], but EtoP connections also occur in other systems [18, 23, 42, 48]. For PtoP connections, on the other hand, all examples considered so far in [18, 24, 42, 48] are of codimension zero. Since the dimensions k and l of $W^u(\Gamma_1)$ and $W^s(\Gamma_2)$, respectively, are at least two, finding a PtoP connection of codimension $d \geq 1$ requires a phase space of dimension $n \geq 4$. Furthermore, Q must be a PtoP heteroclinic connection, that is, $\Gamma_1 \neq \Gamma_2$. Hence, the minimal example of a PtoP connecting orbit that is not structurally stable requires $n = 4$, $k = 2$ and $l = 2$ so that the connection (if it exists) is of codimension $d = 1$.

It is not a straightforward task to find a vector field with the required overall properties. We proceed by identifying a bifurcation structure in parameter space near which one expects to find two suitable periodic orbits. More specifically, we propose to look in a two-dimensional parameter space near a curve of saddle-node of limit cycles bifurcations that create Γ_1 and Γ_2 as saddle objects in \mathbb{R}^4 . Then, say, Γ_1 has a two-dimensional unstable manifold and a three-dimensional stable manifold, while Γ_2 has a two-dimensional stable manifold and a three-dimensional unstable manifold. Furthermore, the two-dimensional manifold $Q_0 = W^s(\Gamma_1) \cap W^u(\Gamma_2)$ is a topological cylinder that is bounded by Γ_1 and Γ_2 . In other words, Γ_1 and Γ_2 have the correct ‘local’ properties. The main question is, hence, whether the two-dimensional manifolds $W^u(\Gamma_1)$ and $W^s(\Gamma_2)$ are ‘close enough’ to each other, so that they may pass through each other (along a suitable path in the two-dimensional parameter space). If they do then the codimension-one PtoP connection Q_1 also

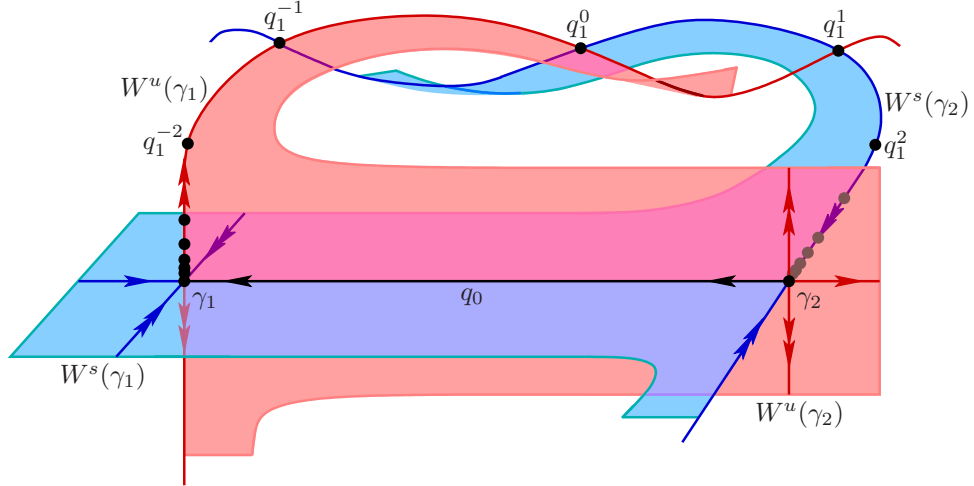


Figure 1: Schematic of the global structure of a codimension-one PtoP heteroclinic cycle in \mathbb{R}^4 near a saddle-node bifurcation of the two periodic orbits Γ_1 and Γ_2 , sketched on the level of a three-dimensional (local) Poincaré section Σ_{cyl} transverse to Γ_1 and Γ_2 . The two corresponding saddle fixed points γ_1 and γ_2 have a codimension-one connection $q_1 = \{\dots q_1^{-2}, q_1^{-1}, q_1^0, q_1^1, q_1^2, \dots\} = W^u(\gamma_1) \cap W^s(\gamma_2)$ and a codimension-zero connection $q_0 = W^s(\gamma_1) \cap W^u(\gamma_2)$.

exists and the heteroclinic cycle is complete at the corresponding isolated point λ^* along the parameter path.

This situation is best pictured in a three-dimensional (local) Poincaré section Σ_{cyl} transverse to the flow on the cylinder \mathcal{Q}_0 that is bounded by Γ_1 and Γ_2 . Figure 1 shows the saddle fixed points $\gamma_1 = \Gamma_1 \cap \Sigma_{\text{cyl}}$ and $\gamma_2 = \Gamma_2 \cap \Sigma_{\text{cyl}}$ and their invariant global manifolds. Notice the structurally stable one-dimensional heteroclinic connection $q_0 = W^u(\gamma_2) \cap W^s(\gamma_1) = \mathcal{Q}_0 \cap \Sigma_{\text{cyl}}$ from γ_2 to γ_1 . The phase portrait shown corresponds to $\lambda = \lambda^*$ where the PtoP heteroclinic cycle is complete. This means that the one-dimensional manifolds $W^u(\gamma_1)$ and $W^s(\gamma_2)$ intersect in a heteroclinic orbit $q_1 = \{\dots q_1^{-2}, q_1^{-1}, q_1^0, q_1^1, q_1^2, \dots\} = \mathcal{Q}_1 \cap \Sigma_{\text{cyl}}$; under the Poincaré return map on Σ_{cyl} points in q_1 move to γ_1 and γ_2 under backward and forward iteration, respectively. When a generic parameter $\lambda \in \mathbb{R}$ is moved through $\lambda = \lambda^*$ then $W^u(\gamma_1)$ and $W^s(\gamma_2)$ pass through each other as curves in \mathbb{R}^3 . Notice further from Fig. 1 that the curve $W^u(\gamma_1)$ bounds the surface $W^u(\gamma_2)$ and the curve $W^s(\gamma_2)$ bounds the surface $W^s(\gamma_1)$.

We remark that the heteroclinic cycle between the two saddle points γ_1 and γ_2 that is shown in Fig. 1 constitutes the minimal example of a heterodimensional cycle of a diffeomorphism on \mathbb{R}^3 . More specifically, in the notation of [8, 9, 17], it is the case of a codimension-one heterodimensional cycle that is quasi-transversal (the tangent spaces of the respective stable and unstable manifolds of γ_1 and γ_2

intersect minimally), connected and non-critical. It has been proved (under an additional small distortion condition) that there are robust non-hyperbolic transitive sets in a parameter neighborhood of such a codimension-one heterodimensional cycle; see [9] and further references therein. The authors of [2, 39] speak of heteroclinic cycles with unstable dimension variability. The transition through a codimension-one heteroclinic cycle as in Fig. 1 is referred to as a crossing bifurcation in [39], where it is shown that it may result in a crisis bifurcation of an attractor. Finding a minimal codimension-one PtoP heteroclinic cycle, hence, provides a concrete example of a minimal heterodimensional cycle and the associated crossing bifurcation. Nearby dynamics can then be investigated in its suspended form in the vector field model, or by considering the local Poincaré map to a section transverse to the periodic orbits.

3 Finding a codimension-one PtoP connection with Lin's method

The mathematical setup of Lin's method for a PtoP connecting orbit Q is a direct generalization of the corresponding setup for an EtoP orbit when the role of the saddle equilibrium is played by another saddle periodic orbit; compare with [42]. Consider a cross-section Σ (an $(n - 1)$ -dimensional submanifold) that intersects Q transversely and separates Γ_1 and Γ_2 . In many situations such a section can be found in the convenient linear form

$$\Sigma = \{x \in \mathbb{R}^n \mid \langle x - p_\Sigma, n_\Sigma \rangle = 0\}, \quad (2)$$

where p_Σ is a point in Σ and n_Σ is a fixed normal vector to Σ . Note that transversality of the flow of (1) to Σ can be assured in practice at least locally near Q , even when Q is not yet known. We now consider the parameter neighborhood Λ of λ^* and define for all $\lambda \in \Lambda$ (λ -dependent) orbit segments

$$Q^- = \{q^-(t) \mid t \leq 0\} \subset W^u(\Gamma_1) \quad \text{where} \quad q^-(0) \in \Sigma, \quad (3)$$

$$Q^+ = \{q^+(t) \mid t \geq 0\} \subset W^s(\Gamma_2) \quad \text{where} \quad q^+(0) \in \Sigma, \quad (4)$$

from Γ_1 to Σ and from Σ to Γ_2 , respectively.

The main idea of Lin's method [45] is that the difference of the points $q^-(0), q^+(0) \in \Sigma$ can be required to lie in a fixed d -dimensional linear subspace Z , which is referred to as the Lin space. There is an element of choice (which we will exploit in what follows), but Z must satisfy the genericity condition

$$(L) \quad \dim(W^+ \oplus W^- \oplus Z) = \dim(\Sigma) = n - 1, \quad \text{where} \quad W^- = T_{Q \cap \Sigma} W^u(\Gamma_1) \cap T_{Q \cap \Sigma} \Sigma \\ \text{and} \quad W^+ = T_{Q \cap \Sigma} W^s(\Gamma_2) \cap T_{Q \cap \Sigma} \Sigma.$$

In other words, in the tangent space $T_{Q \cap \Sigma} \Sigma$ of Σ at $Q \cap \Sigma$ the d -dimensional space Z must span the d -dimensional complement of the sum $W^+ \oplus W^-$ of the respective

tangent spaces of the global manifolds. Since the flow is transverse to Σ , this means that no non-zero vector in Z is allowed to lie in the tangent space of either $W^u(\Gamma_1)$ or $W^s(\Gamma_2)$. Note that for a linear section Σ of the form (2) $T_{Q \cap \Sigma} \Sigma$ is simply the orthogonal complement of n_Σ . A well-known choice for the Lin space Z , which is ‘most transverse’ in a way, is to consider solutions of the adjoint variational equation along Q [36, 46, 52].

Statement of Lin’s method for PtoP orbits. Suppose that system (1) has a PtoP connection Q satisfying conditions (C1)–(C5), and let Z be a d -dimensional space satisfying condition (L) with basis z_1, \dots, z_d . Then, in some neighbourhood Λ of λ^* , for any $\lambda \in \Lambda$ the solutions Q^- and Q^+ as defined by (3) and (4) are uniquely defined by the condition that

$$\xi(\lambda) := q^+(0) - q^-(0) \in Z.$$

Furthermore, there are d smooth functions $\eta_i : \mathbb{R}^m \rightarrow \mathbb{R}$ such that

$$\xi(\lambda) = \sum_{i=1}^d \eta_i(\lambda) z_i \quad \text{and} \quad \eta_i(\lambda^*) = 0 \quad \text{for all } i = 1, \dots, d.$$

This statement is typical for any setup of Lin’s method. The underlying idea is to consider so-called Lin orbits, which may consist of any number of orbit segments with ‘jumps’ in suitable Lin spaces from one orbit segment to the next; see, for example, [36, 50, 52, 54]. Each such Lin orbit is well defined, and it encodes a type of global orbit of interest. When all jumps, that is, all Lin gaps, are zero then one has found the desired global orbit. This approach can be used to study EtoP and PtoP connections, as well as more general heteroclinic networks involving periodic orbits; see [35, 37, 49, 50] for details.

The main step in proving the statement of Lin’s method for PtoP orbits as stated here is to show the uniqueness of the orbit segments Q^- and Q^+ for any $\lambda \in \Lambda$. The properties of the functions η_i are a consequence of this uniqueness. Since the matrix $D\xi$ is non-singular due to condition (C5), the $\eta_i(\lambda)$ — which we refer to as the Lin gaps — are well-defined test functions with regular roots, including a joint regular root at λ^* . An approach to finding an unknown PtoP connection Q is, therefore, to continue the λ -dependent orbit segments Q^- and Q^+ in parameters until all Lin gaps $\eta_i(\lambda)$ are zero.

This Lin’s method setup is sketched in Fig. 2 for the lowest-dimensional case of a codimension-one heteroclinic PtoP connection in \mathbb{R}^4 with $k = l = 2$; then the Lin space Z is of dimension one, and the PtoP connection can be found at an isolated point λ^* of a single parameter $\lambda \in \mathbb{R}$. The situation in panel (a) is for λ near λ^* . The two-dimensional manifolds $W^u(\Gamma_1)$ and $W^s(\Gamma_2)$ of the periodic orbits Γ_1 and Γ_2 are shown up to the three-dimensional section Σ , which they intersect in one-dimensional curves (shown here as two circles). The orbit segments $Q^- \subset W^u(\Gamma_1)$ and $Q^+ \subset W^s(\Gamma_2)$ end in Σ . The difference of their end points

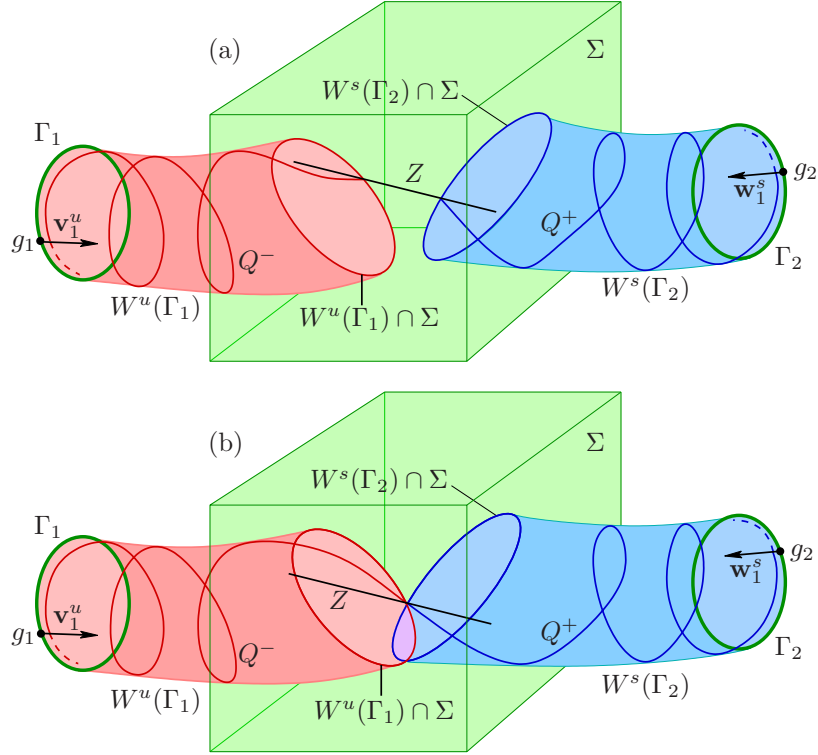


Figure 2: Schematic diagram illustrating the Lin's method setup for finding a codimension-one PtoP connecting orbit in \mathbb{R}^4 . The end points of the two orbit segments, $Q^- \in W^u(\Gamma_1)$ and $Q^+ \in W^s(\Gamma_2)$, in the three-dimensional section Σ lie in the one-dimensional Lin space Z . In the numerical implementation Q^- and Q^+ are truncated to orbit segments whose other end points lie on vectors \mathbf{v}_1^u and \mathbf{w}_1^s in the respective (un)stable eigenspaces at points $g_1 \in \Gamma_1$ and $g_2 \in \Gamma_2$, respectively. Panel (a) shows a non-zero Lin gap along Z for λ near λ^* , and panel (b) shows the PtoP connection $Q = Q^- \cup Q^+$ for $\lambda = \lambda^*$.

$q^+(0)$ and $q^-(0)$ lies along the one-dimensional Lin space Z , giving rise to the single Lin gap $\eta_1(\lambda) = q^+(0) - q^-(0) \neq 0$; for definiteness, we choose the sign of the Lin direction vector z_1 in such a way that $\eta_1(\lambda)$ is initially positive. While Q^- and Q^+ are continued in the parameter λ , the Lin gap $\eta_1(\lambda)$ can be monitored. As is shown in Fig. 2(b), at λ^* the orbit segments Q^- and Q^+ meet and form the PtoP connecting orbit Q . Note that $\eta_1(\lambda)$ undergoes a sign change at λ^* because it is a regular root.

3.1 Implementation of the method

The continuation of families of orbit segments is a very powerful and accurate general numerical method for the investigation of global objects in dynamical systems such as invariant manifolds, connecting orbits and slow manifolds; see [1, 20, 41] for more details. The key step is to formulate a suitable parameterized family of well-posed BVPs, which can be solved, for example, with the collocation solver of the package AUTO [21]. Solutions of the BVP can then be continued in parameters with AUTO's pseudo-arclength continuation routine. In this spirit, the setup of Lin's method presented in the previous section can be implemented numerically by defining a boundary value problem (BVP) for all the objects involved, namely, for finite-time approximations \mathbf{u}^- of Q^- and \mathbf{u}^+ of Q^+ , as well as for the periodic orbits Γ_1 and Γ_2 and their linear (un)stable eigenfunctions. For the convenient definition of orbit segments, one considers (1) in the rescaled version

$$\mathbf{u}'(t) = T f(\mathbf{u}(t), \lambda), \quad (5)$$

where $T \in \mathbb{R}$ is a parameter. Then any orbit segment satisfying (5) can be considered in the standard form

$$\mathbf{u} : [0, 1] \mapsto \mathbb{R}^n$$

over the time interval $[0, 1]$, where the actual integration time in (1) appears as the explicit parameter T . The finite-time approximations \mathbf{u}^- of Q^- and \mathbf{u}^+ of Q^+ can now be defined as solutions of the BVP

$$(\mathbf{u}^-)'(t) = T^- f(\mathbf{u}^-(t), \lambda), \quad (6)$$

$$(\mathbf{u}^+)'(t) = T^+ f(\mathbf{u}^+(t), \lambda), \quad (7)$$

$$\mathbf{u}^-(0) = g_1 + \sum_{i=1}^{k-1} \varepsilon_i \mathbf{v}_i^u, \quad (8)$$

$$\mathbf{u}^+(1) = g_2 + \sum_{i=1}^{l-1} \delta_i \mathbf{w}_i^s, \quad (9)$$

$$\langle \mathbf{u}^-(1) - p_\Sigma, n_\Sigma \rangle = 0, \quad (10)$$

$$\mathbf{u}^+(0) - \mathbf{u}^-(1) = \sum_{i=1}^d \eta_i z_i. \quad (11)$$

Boundary conditions (6) and (7) define \mathbf{u}^- and \mathbf{u}^+ as orbit segments with integration times T^- and T^+ , respectively. Conditions (8) and (9) are projection boundary conditions [4, 5] near the periodic orbits Γ_1 and Γ_2 , which require that the start point of \mathbf{u}^- and the end point of \mathbf{u}^+ lie in the respective linear eigenspaces $E^u(\Gamma_1)$ and $E^s(\Gamma_2)$ (or Floquet vector bundles). Here, $g_1 \in \Gamma_1$ is a chosen point, $\mathbf{v}_i^u \in E^u(\Gamma_1)$, $1 \leq i \leq k-1$ are the unstable Floquet vectors of Γ_1 at g_1 , and the $k-1$ coefficients $\varepsilon_i \in \mathbb{R}$ are parameters of the BVP. Similarly, $g_2 \in \Gamma_2$ is a chosen point, $\mathbf{w}_i^s \in E^s(\Gamma_2)$,

$1 \leq i \leq l - 1$ are the stable Floquet vectors of Γ_2 at g_2 , and the $l - 1$ coefficients $\delta_i \in \mathbb{R}$ are parameters of the BVP. Boundary conditions (10) and (11) ensure that the difference between the end points $\mathbf{u}^-(1)$ and $\mathbf{u}^+(0)$ lies in the Lin space Z ; here Z is spanned by the vectors z_1, \dots, z_d , and the coefficients η_i describe the difference in this basis.

The formulation of (6)–(11) is quite compact and shows that this BVP for \mathbf{u}^- and \mathbf{u}^+ is well posed. More specifically, the orbits (6)–(7) are given by a system of $N = 2n$ equations, while (8)–(11) are a system of $B = 3n + 1$ constraints. Hence, for any fixed value of the parameter λ there is a unique solution for the $B - N = n + 1 = 2 + (k - 1) + (l - 1) + d$ internal parameters $T^-, T^+, \varepsilon_i, \delta_i$ and η_i . When solutions of the BVP (6)–(11) are continued, the periodic orbits Γ_i and their unstable and stable eigenfunctions need to be continued simultaneously as solutions of separate well-posed BVPs; see, for example, [20, 23, 42] for more details. The periodic orbits are represented as the solutions \mathbf{u}_{Γ_i} of

$$(\mathbf{u}_{\Gamma_i})'(t) = T_{\Gamma_i} f(\mathbf{u}_{\Gamma_i}(t), \lambda), \quad (12)$$

$$\mathbf{u}_{\Gamma_i}(0) = \mathbf{u}_{\Gamma_i}(1), \quad (13)$$

$$\int_0^1 \langle \dot{\mathbf{u}}_{\Gamma_i}, \mathbf{u}_{\Gamma_i}(\tau) \rangle d\tau = 0. \quad (14)$$

Here $T = T_{\Gamma_i}$ is the (minimal) period of Γ_i and (14) is a standard integral phase condition [20]. The solutions \mathbf{u}_{Γ_i} are found in practice by continuation, for example, from a Hopf bifurcation. Numerical representations $\mathbf{u}_i^{u/s}$ of the unstable and stable eigenfunctions of Γ_1 and Γ_2 , respectively, can be obtained as the solutions of

$$(\mathbf{u}_i^{u/s})'(t) = T_{\Gamma_i} D_u f(\mathbf{u}_{\Gamma_i}(t), \lambda) \mathbf{u}_i^{u/s}(t), \quad (15)$$

$$\mathbf{u}_i^{u/s}(1) = \mu_i^{u/s} \mathbf{u}_i^{u/s}(0), \quad (16)$$

$$\langle \mathbf{u}_i^{u/s}(0), \mathbf{u}_i^{u/s}(0) \rangle = 1. \quad (17)$$

Here the $\mu_i^{u/s}$ are the respective Floquet multipliers of Γ_1 and Γ_2 , which can be found as branch points of an initial continuation run of the trivial bundle. A second run then increases the norm in (17) from zero; see [15, 23, 26, 42] for more details. With these representations one sets $g_1 = \mathbf{u}_{\Gamma_1}(0)$ and obtains the required unstable Floquet vectors as $\mathbf{v}_i^u = \mathbf{u}_i^u(0)$, ($i = 1, \dots, k - 1$) in (8), and similarly for $g_2 = \mathbf{u}_{\Gamma_2}(0)$ and the stable Floquet vectors $\mathbf{w}_i^s = \mathbf{u}_i^s(0)$, ($i = 1, \dots, l - 1$) in (9).

In order to find initial orbit segments \mathbf{u}^- and \mathbf{u}^+ that satisfy the BVP (6)–(11) one proceeds as follows. First, one determines, for a suitable and fixed value of the system parameter λ , the two periodic orbits Γ_1 and Γ_2 and their linear eigenfunctions. One then defines the section Σ , for example, as in (2). To find an orbit segment \mathbf{u}^- that ends in Σ , one considers the BVP given by (6) and (8) for fixed small ε_i . Starting from a small positive value, one continues the solution family in T^- (effectively, solving the initial value problem), which grows the orbit \mathbf{u}^- from near Γ_1 until Σ is reached; this can be detected by monitoring $\langle \mathbf{u}^-(1) - p_\Sigma, n_\Sigma \rangle$ until

a zero is detected. Similarly, an orbit segment \mathbf{u}^+ that starts in Σ can be found by continuing solutions of the BVP given by (7) and (9) for fixed small δ_i in T^+ while monitoring $\langle \mathbf{u}^+(0) - p_\Sigma, n_\Sigma \rangle$. After these continuation runs we have $\mathbf{u}^-(1) \in \Sigma$ and $\mathbf{u}^+(0) \in \Sigma$, and we can define the Lin space Z as a space that contains the difference by setting $z_1 = (\mathbf{u}^+(0) - \mathbf{u}^-(1)) / \|\mathbf{u}^+(0) - \mathbf{u}^-(1)\|$ for this fixed value of the parameter λ . Generically, with this choice the space Z satisfies condition (L) and the η_i can be determined after the remaining basis vectors z_2, \dots, z_d have been chosen; see also [42]. In particular, for the case $d = \dim(Z) = 1$, which is considered in the subsequent sections, one has in (11) that $Z = \text{span}(z_1)$ and $\eta_1 = \mathbf{u}^+(0) - \mathbf{u}^-(1)$. It is important to note that, once chosen, the Lin space Z and its basis vectors z_i remain fixed.

The orbit segments \mathbf{u}^- and \mathbf{u}^+ obtained in this way satisfy (6)–(11). Hence, one can now continue \mathbf{u}^- and \mathbf{u}^+ in the system parameter λ to find the desired heteroclinic connection of codimension d as a joint zero of the test functions η_i , ($i = 1, \dots, d$). As was already mentioned, this requires the simultaneous continuation in λ of $g_1 = \mathbf{u}_{\Gamma_1}(0)$, \mathbf{v}_i^u , $g_2 = \mathbf{u}_{\Gamma_2}(0)$ and \mathbf{w}_i^s in (8) and (9) as solutions of BVPs (12)–(14) and (15)–(17); this can be achieved with the package AUTO by considering the single combined BVP (6)–(17). Once a PtoP connection has been found in this way, it can be continued in (further) system parameters, as will be presented in Sec. 5.

4 A simple model of intracellular calcium dynamics.

In this section we specify a model of intracellular calcium dynamics and show that it has the geometric elements required for the existence of a codimension-one PtoP heteroclinic cycle with $n = 4$ and $d = 1$. In the next section we will locate this global bifurcation and follow its bifurcation locus in a two-dimensional parameter space.

4.1 Model description

The model we consider is based on the Atri model of intracellular calcium oscillations [3]. In the Atri model, oscillations in the concentration of free cytoplasmic calcium arise through sequential release of calcium from the endoplasmic reticulum (ER) through inositol trisphosphate receptors (IPR) and uptake of calcium to the ER through ATPase pumps. Calcium can also enter and leave the cell from the outside. Details about the modeling assumptions that give rise to the original Atri model can be found in [3] and [32]. We are interested in a traveling wave version of the Atri model, which is obtained by including a diffusion term in the Atri model and then transforming to a moving frame. A general discussion of traveling wave equations for calcium models is contained in [10], with a comprehensive review of models of calcium waves being given in [27]. Our simplified model keeps the essential qualitative features of the original Atri model, but uses much simpler functional forms for the various fluxes. A discussion of the steps taken in simplifying the fluxes

α	k_s	k_f	k_p	φ_1	φ_2	τ	γ	D_c	δ
0.05 s^{-1}	20.0 s^{-1}	20.0 s^{-1}	20.0 s^{-1}	$2.0 \text{ } \mu\text{M}$	$1.0 \text{ } \mu\text{M}$	2.0 s^{-1}	5.0	25.0	0.2

Table 1: Parameters of the simplified Atri model, equations (18).

is given in [55].

The equations for the simplified Atri model are:

$$\begin{aligned}
\dot{c} &= d, \\
D_c \dot{d} &= sd - \left(\left(\alpha + \frac{k_f c^2}{c^2 + \varphi_1^2} n \right) \left(\frac{\gamma(c_t + D_c d - sc)}{s} - c \right) - k_s c + \delta(J_{\text{in}} - k_p c) \right), \\
\dot{c}_t &= \delta(J_{\text{in}} - k_p c), \\
s \dot{n} &= \frac{1}{\tau} \left(\frac{\varphi_2}{\varphi_2 + c} - n \right).
\end{aligned} \tag{18}$$

Here, c represents the concentration of free calcium in the cytosol, c_t is the total number of moles of calcium in the cell, divided by the cytoplasmic volume, and n is the proportion of IPR that have not been inactivated by calcium. The parameter δ represents the magnitude of fluxes through the cell membrane relative to the fluxes through the ER membrane, the diffusion coefficient of cytoplasmic calcium is denoted by the parameter D_c , and the ratio between the volume of the ER and the volume of the cytoplasm is denoted by the parameter γ . The terms $k_s c$ and $k_p c$ represent the calcium fluxes pumped from the cell cytoplasm into the ER and out of the cell, respectively. The term

$$\left(\alpha + \frac{k_f c^2}{c^2 + \varphi_1^2} n \right) \left(\frac{\gamma(c_t + D_c d - sc)}{s} - c \right)$$

represents the calcium flux from the ER into the cytoplasm, while the term J_{in} represents the calcium flux going into the cell cytoplasm from outside the cell. In the analysis that follows, J_{in} is one of the main bifurcation parameters, with the other bifurcation parameter being s , the wave speed of calcium waves. The values of the other model parameters are given in Table 1.

4.2 Partial bifurcation study

As discussed in [10], a wide variety of models of intracellular calcium waves and other excitable systems have a common basic bifurcation structure if the model is formulated in traveling wave coordinates: there is a C-shaped curve of homoclinic bifurcations (corresponding to traveling pulse solutions in the underlying PDE) and a U-shaped curve of Hopf bifurcations (corresponding to the onset of periodic waves in the underlying PDE). In [10], this kind of system is called a ‘CU system’.

Panel (a) of Fig. 3 shows the CU bifurcation structure that occurs in the (J_{in}, s) parameter plane for the simplified Atri model (18). Equations (18) have a single

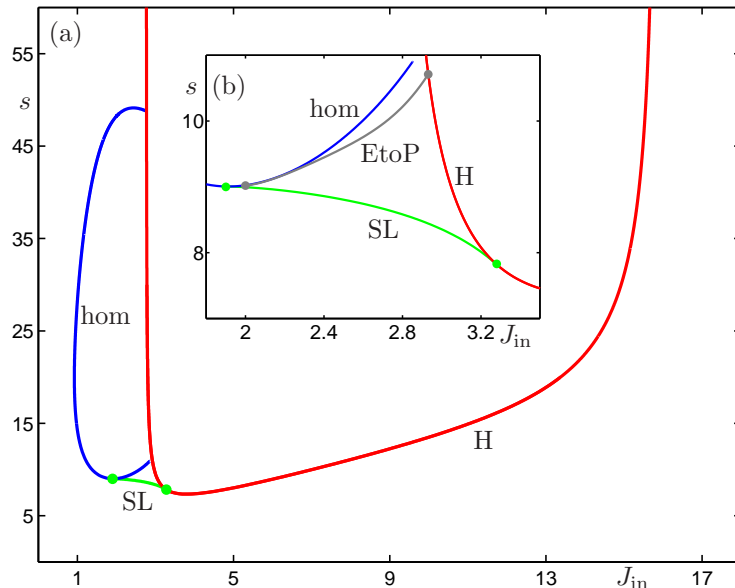


Figure 3: Panel (a) shows a partial bifurcation set in the (J_{in}, s) -plane for equations (18), consisting of a C-shaped curve (labeled hom) of homoclinic bifurcations and a U-shaped curve (labeled H) of Hopf bifurcations, which are connected by a curve of saddle-node of limit cycles bifurcations (labeled SL). Panel (b) is an enlargement near the curve SL, and also shows a curve of EtoP connections with end points on the curves H and hom.

equilibrium solution p , which is always of saddle type, having one negative eigenvalue and three eigenvalues with positive real parts inside the region bounded by the Hopf curve (labeled H), and having one positive eigenvalue and three eigenvalues with negative real parts outside this region. The equilibrium undergoes a supercritical Hopf bifurcation on the section of the Hopf locus to the left of a codimension-two degenerate Hopf bifurcation marked by a dot, and undergoes a subcritical Hopf bifurcation on the rest of the Hopf curve.

The curve of homoclinic bifurcations of p is labeled hom in Fig. 3. The upper end of this curve terminates on the Hopf curve at a codimension-two Shil'nikov-Hopf bifurcation [14, 33]. The lower end of the homoclinic curve does not actually reach the Hopf bifurcation curve H. Instead it has a sharp turning point and traces back very close to itself, stopping at a codimension-two Belyakov bifurcation point where the saddle-quantity of the equilibrium is equal to zero. Complex dynamics are known to arise in the neighbourhood of such a Belyakov point [44]. Figure 3 shows a curve SL of saddle-node of limit cycles bifurcations that emerges from this

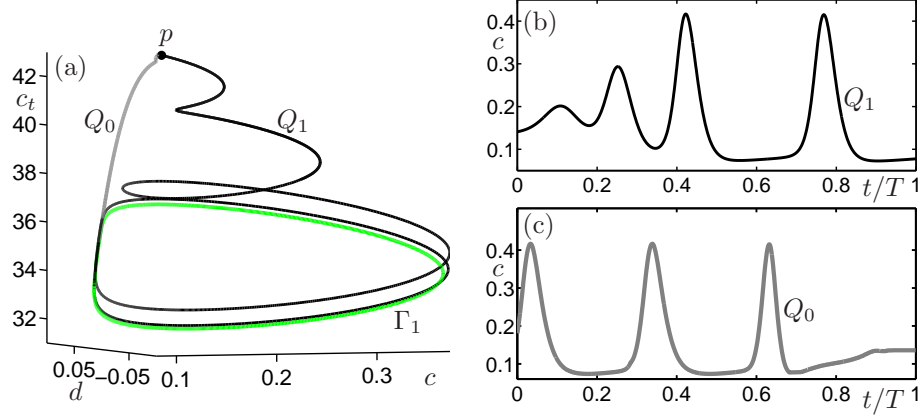


Figure 4: Panel (a) shows the EtoP cycle for $s = 10.0$ and $J_{\text{in}} = 2.71917$ between the equilibrium p and the periodic orbit Γ_1 , which consists of the codimension-one EtoP connection Q_1 and the codimension-zero EtoP connection Q_0 . Time traces (of the variable c) of the computed orbit segments Q_1 and Q_0 are shown in panels (b) and (c), respectively.

point and ends at the degenerate Hopf point on curve H.

In the region of the (J_{in}, s) -plane between the curves H and SL, which is shown enlarged in Fig. 3(b), there exist two saddle-type periodic orbits, Γ_1 and Γ_2 , that are created in a pair along the curve SL. We seek a codimension-one heteroclinic cycle between these two periodic orbits in this region of parameter space, and observe that Γ_1 and Γ_2 have the correct ‘local’ properties; see the discussion in Sec. 2.1. Specifically, they have stable and unstable manifolds, respectively, of dimension three, which must intersect (locally near the curve SL) in a two-dimensional cylinder that lies in the center manifold of the saddle-node of limit cycles bifurcation.

A hint that there may be a codimension-one PtoP heteroclinic cycle in this system comes from Fig. 4, which shows a codimension-one EtoP heteroclinic cycle connecting the saddle equilibrium p and the saddle periodic orbit Γ_1 . The two connecting orbits Q_0 and Q_1 were found with the Lin’s method setup from Ref. [42] as implemented in the AUTO. The connection Q_1 from p to Γ_1 is of codimension one, and it occurs when the one-dimensional unstable manifold $W^u(p)$ lies in the three-dimensional stable manifold $W^s(\Gamma_1)$; see Fig. 4(a) and the time series of the variable c along Q_1 in panel (b). There also exists a structurally stable heteroclinic connection from Γ_1 back to p , which is the intersection of the two-dimensional unstable manifold $W^u(\Gamma_1)$ with the three-dimensional stable manifold $W^s(p)$; see Fig. 4(a) and the time series along Q_0 in panel (c). Once it was found as the solution of the corresponding BVP from [42], the locus of codimension-one EtoP connections was continued to yield the curve labeled EtoP in Fig. 3(b). This curve has one end point at $(J_{\text{in}}, s) = (2.93121, 10.51284)$ on the Hopf bifurcation curve and another end point at $(J_{\text{in}}, s) =$

(2.04216, 9.04523) on the homoclinic bifurcation curve (near the Belyakov point). In the region of interest we also find the second periodic orbit Γ_2 , which bifurcates from the curve H in Fig. 3(b) and, hence, is quite close to the equilibrium p . Therefore, the existence of the EtoP connections from p to Γ_1 and back strongly suggests that there may also be a PtoP cycle between Γ_1 and Γ_2 . Overall, we conclude that the global geometry of the phase space of (18) looks very promising for the hunt for a codimension-one PtoP cycle with the method from Sec. 3.1.

5 Finding the codimension-one PtoP cycle in the simplified Atri model

In this section we describe the computations needed to locate a codimension-one PtoP cycle in the Atri model and then to follow the locus of the bifurcation in the (J_{in}, s) parameter plane. All computations of solution families of BVPs are implemented and performed with the AUTO07p release of the package AUTO, which uses orthogonal collocation with Gauss-Legendre polynomials [20, 21]. Throughout we use polynomials of degree $NCOL = 4$ in each collocation interval and, depending on the complexity of the orbit, between $NTST = 100$ and $NTST = 1000$ collocation intervals. Note that all boundary value problems, for the periodic orbits, their (un)stable eigenfunctions and for the orbit segments Q^- and Q^+ , are represented in AUTO07p over the same mesh as specified by $NTST$ and $NCOL$; see also [42].

To start, we fix $s = 9.0$ and continue two periodic orbits Γ_1 and Γ_2 of (18) for decreasing J_{in} from the Hopf bifurcation points at $J_{\text{in}} = 6.04467$ and at $J_{\text{in}} = 3.04800$, where they are born, respectively. Inspection of the Floquet multipliers shows that Γ_1 has a two-dimensional unstable manifold and a three-dimensional stable manifold, while Γ_2 has a three-dimensional unstable manifold and a two-dimensional stable manifold. The continuation of Γ_1 and Γ_2 is stopped at $J_{\text{in}} = 3.0$, which is a point right in the region of interest; see Fig. 3(b). We now compute the eigenfunctions of Γ_1 and Γ_2 by setting up BVP (15)–(17) for both periodic orbits. Furthermore, we define the section

$$\Sigma = \{(c, d, c_t, n) \mid c_t = 36.0\},$$

for which $p_\Sigma = (0, 0, 36, 0)$ and $n_\Sigma = (0, 0, 1, 0)$ in (2). The section Σ divides the phase space of (18) into two parts, one containing Γ_1 (where $c_t < 36.0$) and the other containing Γ_2 (where $c_t > 36.0$). It is important to realize that any orbit connecting Γ_1 and Γ_2 must cross Σ .

5.1 The codimension-one PtoP connection

We first consider the PtoP connecting orbit Q_1 from Γ_1 to Γ_2 which, if it exists, is of codimension one since $n = 4$, $k = 2$, $l = 2$ and $d = 1$. An initial orbit segment Q_1^- from Γ_1 to the section Σ is found by performing a continuation in the integration time T^- of the BVP (6) and (8) for $g_1 = (0.0915, 0.0019, 34.0078, 0.8833) \in \Gamma_1$, the

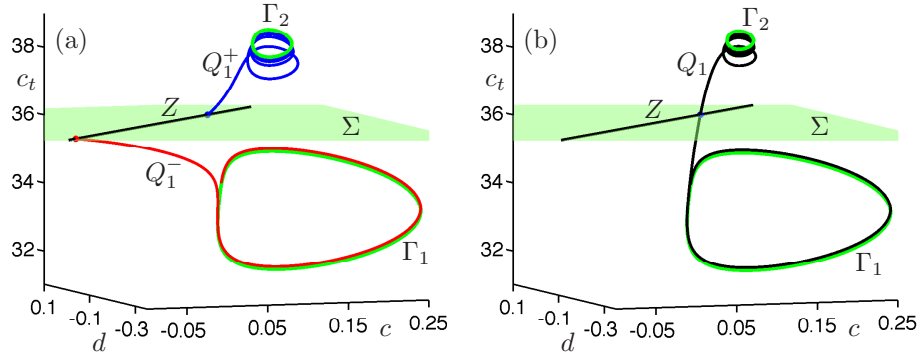


Figure 5: Computing the codimension-one PtoP connection Q_1 for $s = 9.0$. Panel (a) for $J_{\text{in}} = 3.0$ shows two initial orbit segments Q_1^- from Γ_1 to $\Sigma = \{c_t = 36.0\}$ and Q_1^+ from Σ to Γ_2 with a Lin gap in Σ of $\eta_1 = 0.4065$ along the direction Z . Panel (b) shows the connecting orbit Q_1 for $J_{\text{in}} = 3.02661$ where $\eta_1 = 0$.

associated Floquet vector $\mathbf{v}_1^u = (-0.1997, -0.1630, 0.9661, 0.0106)$ of the unstable Floquet multiplier $\mu_1^u = 95340$ and $\varepsilon_1 = 10^{-6}$. Similarly, an orbit segment Q_1^+ from Σ to Γ_2 is found by continuation in T^+ of the BVP (7) and (9), where now $g_2 = (0.1347, 0.0023, 38.2595, 0.8728) \in \Gamma_2$, $\mathbf{w}_1^s = (0.0108, -0.0064, 0.9981, -0.0606)$ is the associated Floquet vector of the stable Floquet multiplier $\mu_1^s = 0.3387$ and $\delta_1 = 10^{-4}$. Figure 5(a) shows the periodic orbits Γ_1 and Γ_2 , the section Σ and the orbit segments Q_1^- and Q_1^+ for $(J_{\text{in}}, s) = (3.0, 9.0)$ in projection onto (c, d, c_t) -space. Also shown is the Lin space Z , which we also refer to as the Lin direction because it is of dimension $d = 1$. It is chosen here as the line through the two end points $Q_1^- \cap \Sigma$ and $Q_1^+ \cap \Sigma$ for $(J_{\text{in}}, s) = (3.0, 9.0)$, and is spanned by a direction vector z_1 ; the initial Lin gap is $\eta_1 = 0.4065$ in Fig. 5(a). We stress that the Lin vector z_1 is kept fixed throughout further computations, that is, it is not allowed to change with system parameters. After these initial computations, the overall BVP (6)–(11), together with BVPs (12)–(14) and (15)–(17) for both Γ_1 and Γ_2 , can be continued in a single system parameter. Specifically, we continue Q_1^- and Q_1^+ as solutions of this overall BVP in the parameter J_{in} and thus detect that $\eta_1 = 0$ for $J_{\text{in}} = 3.02661$. Figure 5(b) depicts the corresponding codimension-one PtoP connection Q_1 from Γ_1 to Γ_2 , which is the concatenation of the two orbit segments Q_1^- and Q_1^+ .

5.2 The codimension-zero PtoP connection

We next find the codimension-zero connection Q_0 from Γ_2 to Γ_1 at $(J_{\text{in}}, s) = (3.02661, 9.0)$. The roles of Γ_1 and Γ_2 are now exchanged in the formulation of the BVP. Furthermore, $n = 4$, $k = 3$ and $l = 3$, so that $W^u(\Gamma_2)$ intersects $W^s(\Gamma_1)$ in a two-dimensional surface. First, we consider an orbit segment Q_0^- whose starting point lies near the base point $g_1 = (0.1405, 0.0020, 38.2727, 0.8708) \in \Gamma_2$ along the as-

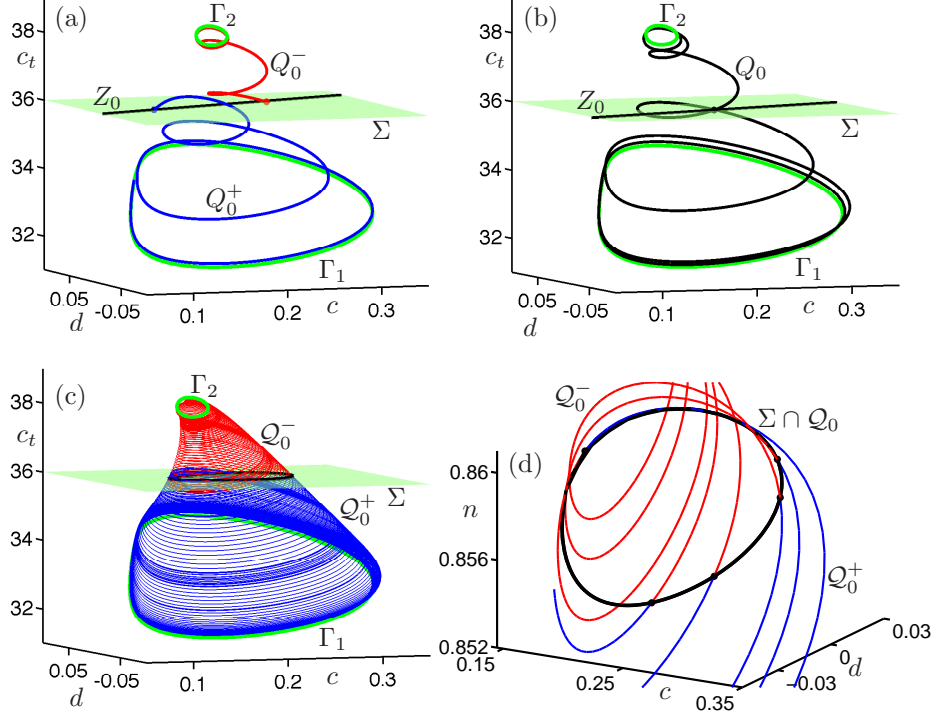


Figure 6: Computing the cylinder \mathcal{Q}_0 of codimension-zero PtoP connections from Γ_2 to Γ_1 for $s = 9.0$ and $J_{\text{in}} = 3.02661$. Panel (a) shows two initial orbit segments Q_0^- from Γ_2 to $\Sigma = \{c_t = 36.0\}$ and Q_0^+ from Σ to Γ_1 with a gap in Σ of $\eta_0 = 0.1624$ along the direction Z_0 . Panel (b) shows a codimension-zero PtoP connecting orbit Q_0 where $\eta_0 = 0$. Panel (c) shows the one-parameter families \mathcal{Q}_0^- and \mathcal{Q}_0^+ that form a cylinder of connecting PtoP orbits, and panel (d) is an enlargement of \mathcal{Q}_0^- and \mathcal{Q}_0^+ near their intersection curve $\mathcal{Q}_0 \cap \Sigma$.

sociated two-dimensional unstable eigenspace $E^u(\Gamma_2)$, which is spanned by Floquet vectors $\mathbf{v}_1^u = (0.8676, -0.3284, 0.1326, -0.3491)$ and $\mathbf{v}_2^u = (-0.1038, -0.0434, 0.9936, 0.0092)$ of the unstable Floquet multipliers $\mu_1^u = 1.3045$ and $\mu_2^u = 695.9515$; initial distances along these vectors are $\varepsilon_1 = 10^{-4}$ and $\varepsilon_2 = 10^{-6}$, respectively. Continuation in the integration time T^- is performed until the end point of Q_0^- lies in the section Σ . Secondly and similarly, we find an orbit segment Q_0^+ whose starting point lies in Σ and whose end point lies near the base point $g_2 = (0.0919, 0.0020, 33.9624, 0.8823) \in \Gamma_1$ in the corresponding two-dimensional stable eigenspace $E^s(\Gamma_1)$, which is spanned by associated Floquet vectors $\mathbf{w}_1^s = (-0.0059, -0.0001, 0.9914, -0.1310)$ and $\mathbf{w}_2^s = (0.2051, -0.1042, 0.9692, 0.0884)$ of the stable Floquet multipliers $\mu_1^s = 0.2757$ and $\mu_2^s = 0.0077$; initial distances along these vectors are $\delta_1 = 10^{-4}$ and $\delta_2 = 10^{-6}$, respectively. The periodic orbits Γ_1 and Γ_2 and the orbit segments Q_0^- and Q_0^+ up

to Σ for $(J_{\text{in}}, s) = (3.02661, 9.0)$ are shown in Fig. 6(a) in projection onto (c, d, c_t) -space. To find an actual PtoP connection we adapt a numerical setup that was first employed in [42]. Specifically, we define the one-dimensional space Z_0 as the direction given by $Q_0^- \cap \Sigma$ and $Q_0^+ \cap \Sigma$, spanned by the vector z_0 . While Z_0 is not a Lin space (in the sense of the Statement of Lin’s method in Sec. 3) it plays a similar role during the computation and remains fixed from now on. More specifically, we consider the BVP (6)–(10) with the additional boundary condition

$$\mathbf{u}^+(0) - \mathbf{u}^-(1) = \eta_0 z_0, \quad (19)$$

where $\eta_0 = 0.1624$ is the initial gap size. The idea is now to continue Q_0^- and Q_0^+ as solutions of this BVP with the gap size η_0 as the main continuation parameter, while the system parameters, J_{in} and s , remain fixed. This continuation for fixed $(J_{\text{in}}, s) = (3.02661, 9.0)$ yields a zero of η_0 , which corresponds to the connecting orbit Q_0 shown in Fig. 6(b).

In fact, the BVP given by (6)–(10) and (19) has a one-dimensional solution manifold, because, for fixed $\eta_0 = 0$, it has only $B - N = n + 1 = 5$ conditions for the six free internal parameters $T^-, T^+, \varepsilon_1, \varepsilon_2, \delta_1, \delta_2$. Hence, a continuation of this BVP with $\eta_0 = 0$ allows us to follow the initial connecting orbit Q_0 (which is not isolated) in internal parameters as it sweeps out the two-dimensional surface \mathcal{Q}_0 of connecting orbits from Γ_2 to Γ_1 . The surface \mathcal{Q}_0 is the topological cylinder bounded by the two periodic orbits that is shown in Fig. 6(c) in projection onto (c, d, c_t) -space. It consists of two bounded cylinders, \mathcal{Q}_0^- from Γ_2 to Σ and \mathcal{Q}_0^+ from Σ to Γ_1 , which connect in the section Σ along the closed curve $\mathcal{Q}_0 \cap \Sigma$. Figure 6(d) shows $\mathcal{Q}_0 \cap \Sigma$ in (c, d, n) -space, together with selected orbit segments of \mathcal{Q}_0^- and \mathcal{Q}_0^+ .

Figure 7 shows the entire PtoP cycle between Γ_1 and Γ_2 for $(J_{\text{in}}, s) = (3.02661, 9.0)$ in projection onto (c, d, c_t) -space. The codimension-one PtoP orbit Q_1 connects Γ_1 to Γ_2 . The connection from Γ_2 back to Γ_1 , on the other hand, consists of a one-parameter family of connecting PtoP orbits (parameterized, for example, by $\mathcal{Q}_0 \cap \Sigma$); it forms the cylinder $\mathcal{Q}_0 = W^u(\Gamma_2) \cap W^s(\Gamma_1)$, which has been rendered in Fig. 7 as a two-dimensional surface. Note that Fig. 7 shows in projection onto (c, d, c_t) -space the same dynamical object that was sketched in Fig. 1 on the level of a Poincaré return map to the three-dimensional local section Σ_{cyl} transverse to the orbits on \mathcal{Q}_0 .

5.3 Continuation of the PtoP cycle

The locus of the codimension-one PtoP heteroclinic connection Q_1 can be continued in the system parameters J_{in} and s as the solution of the BVP (6)–(11) with the additional condition that $\eta_1 = 0$. The resulting curve, labeled PtoP, is shown in Fig. 8. The curve has one end point on the curve of saddle-node of limit cycles bifurcations (SL), then follows the Hopf bifurcation curve (H) closely for increasing s and ends on H; see Fig. 8(b). Along the curve PtoP we also continued a single connecting orbit Q_0 of the family \mathcal{Q}_0 of codimension-zero PtoP connections as the

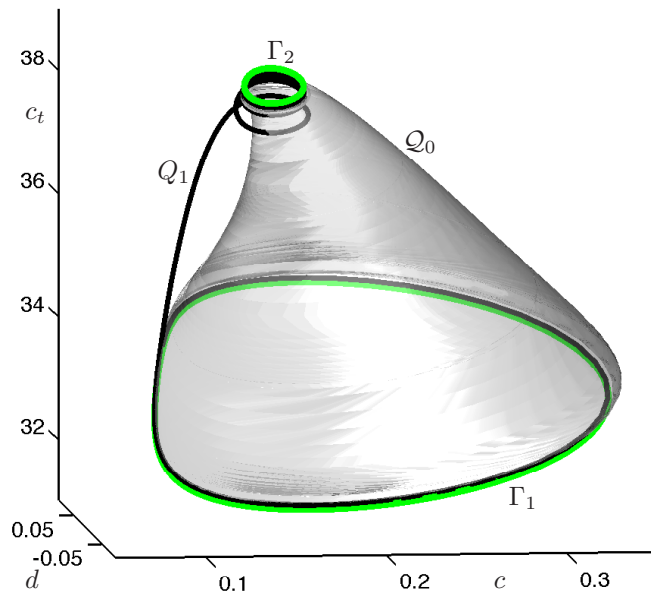


Figure 7: The heteroclinic PtoP cycle between Γ_1 and Γ_2 for $(J_{\text{in}}, s) = (3.02661, 9.0)$, consisting of the codimension-one PtoP connection Q_1 from Γ_1 to Γ_2 and the bounded cylinder Q_0 of PtoP connections from Γ_2 to Γ_1 .

solution of the BVP defined by (6)–(9) and (19) for fixed $\eta_0 = 0$. This computation confirmed that the entire heteroclinic cycle exists along the curve PtoP in Fig. 8.

Figure 9(a) shows the heteroclinic PtoP cycle that one finds when $s = 10.0$, and panel (b) shows the heteroclinic cycle for $s = 8.5$. The surface Q_0 was swept out by continuation of the single orbit Q_0 as in Sec. 5.2. From Fig. 9(a) we observe that the amplitude of Γ_2 becomes quite small when s is increased from $s = 9.0$ and the curve PtoP is close to the Hopf bifurcation curve H . At the end point of the curve PtoP on H , the periodic orbit Γ_2 finally disappears in the Hopf bifurcation of the equilibrium p . We found numerically that this happens at $(J_{\text{in}}, s) = (2.79224, 24.64540)$. When s is decreased from $s = 9.0$ the periodic orbits Γ_1 and Γ_2 approach one another; see Fig. 9(b). Finally, at the end point $(J_{\text{in}}, s) = (2.98015, 8.37696)$ of the curve PtoP on the curve SL , the two periodic orbits Γ_1 and Γ_2 meet and disappear. At this point of codimension two one finds a saddle-node limit cycle $\hat{\Gamma}$ with a two-dimensional center manifold, whose two-dimensional manifolds $W^u(\hat{\Gamma})$ and $W^s(\hat{\Gamma})$ intersect transversely in \mathbb{R}^4 in a single orbit. On the level of the Poincaré return map to the three-dimensional local section Σ_{cyl} transverse to the orbits on Q_0 , this corresponds to the sketch in Fig. 1 where the saddle points γ_1 and γ_2 have moved towards each other to become a saddle-node $\hat{\gamma}$.

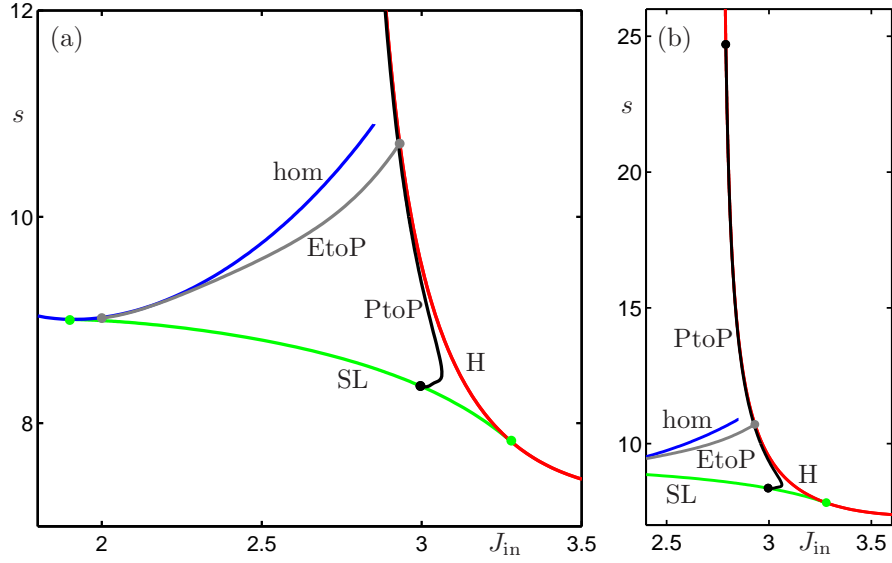


Figure 8: Partial bifurcation set in the (J_{in}, s) -plane of equations (18). This figure shows an enlargement of Fig. 3(a) with the addition of the curve of codimension-one heteroclinic cycles between Γ_1 and Γ_2 (labeled PtoP), which has end points on the saddle-node of limit cycles bifurcation curve SL and on the Hopf bifurcation curve H. Panel (a) shows the region of interest where the PtoP connection was found, and panel (b) shows the entire PtoP curve.

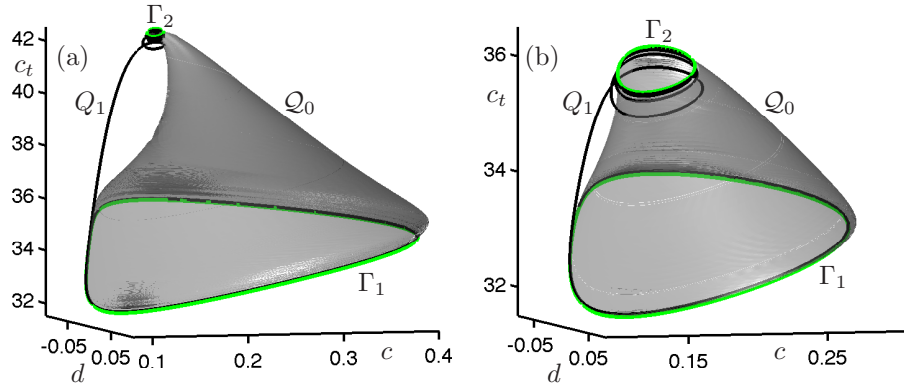


Figure 9: The heteroclinic PtoP cycle between Γ_1 and Γ_2 for $(J_{\text{in}}, s) = (2.95950, 10.0)$ (a) and for $(J_{\text{in}}, s) = (3.06319, 8.5)$ (b); the viewpoint is the same as that in Fig. 7.

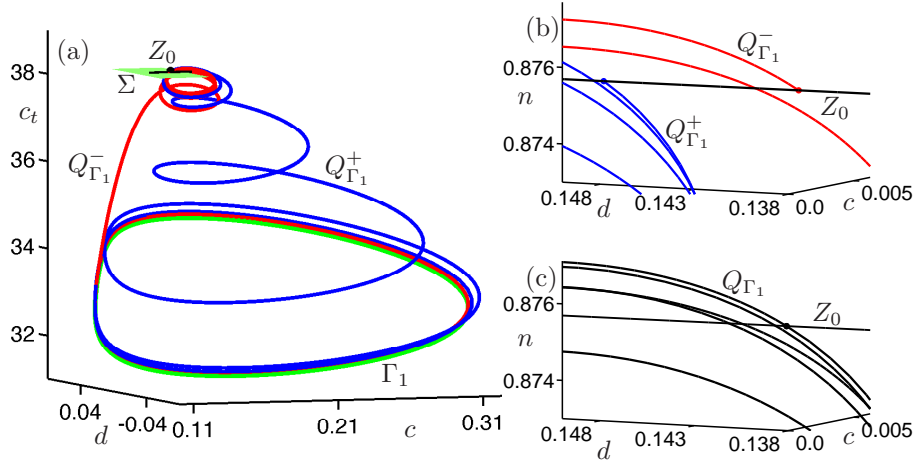


Figure 10: Finding a homoclinic PtoP orbit of Γ_1 via the continuation of orbit segments $Q_{\Gamma_1}^-$ and $Q_{\Gamma_1}^+$ that connect Γ_1 with the section $\Sigma = \{c_t = 38.27\}$. Panel (a) shows the start data for $(J_{\text{in}}, s) = (3.02661, 9.0)$ where $Q_{\Gamma_1}^- = Q_1$ and $Q_{\Gamma_1}^+$ is a connecting orbit in \mathcal{Q}_0 . Panel (b) shows $Q_{\Gamma_1}^-$ and $Q_{\Gamma_1}^+$ near the direction Z_0 in Σ . In panel (c) the gap along Z_0 has been closed, yielding the homoclinic PtoP orbit Q_{Γ_1} .

6 Finding PtoP homoclinic orbits and periodic orbits near the PtoP cycle

In the vicinity of the heteroclinic PtoP cycle between Γ_1 and Γ_2 one can find other dynamical objects, including orbits that are homoclinic to Γ_1 and to Γ_2 and saddle periodic orbits that pass close to Γ_1 and Γ_2 . We now show how these objects can be found numerically with a BVP approach, using the heteroclinic PtoP cycle as start data.

To find a homoclinic orbit connecting Γ_1 to itself we consider two orbit segments: $Q_{\Gamma_1}^-$, which starts near the base point $g_1 \in \Gamma_1$ in the unstable Floquet space and ends at a section Σ near Γ_2 , and $Q_{\Gamma_1}^+$, which starts in Σ and ends near g_1 in the stable Floquet space. These orbit segments are readily available from the knowledge of the PtoP heteroclinic cycle. Specifically, as start data we set $Q_{\Gamma_1}^- = Q_1$ and $Q_{\Gamma_1}^+ \subset \mathcal{Q}_0$. Then the section Σ is chosen to contain the end points of $Q_{\Gamma_1}^-$ and $Q_{\Gamma_1}^+$ near Γ_2 . We define the one-dimensional space Z_0 as the line in Σ through these two end points; the gap η_0 is measured along Z_0 . The setup is the one considered in [42] for the computation of homoclinic PtoP orbits, and $Q_{\Gamma_1}^-$ and $Q_{\Gamma_1}^+$ can be represented by and continued as solutions of the BVP given by (6)–(10) and (19).

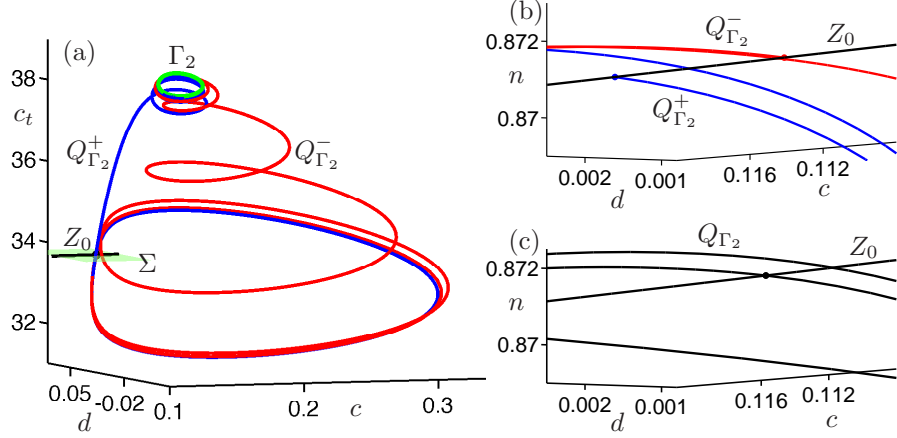


Figure 11: Finding a homoclinic PtoP orbit of Γ_2 via the continuation of orbit segments $Q_{\Gamma_2}^-$ and $Q_{\Gamma_2}^+$ that connect Γ_2 with the section $\Sigma = \{c_t = 33.95\}$. Panel (a) shows the start data for $(J_{\text{in}}, s) = (3.02661, 9.0)$ where $Q_{\Gamma_2}^-$ is a connecting orbit in \mathcal{Q}_0 and $Q_{\Gamma_2}^+ = Q_1$. Panel (b) shows $Q_{\Gamma_2}^-$ and $Q_{\Gamma_2}^+$ near the direction Z_0 in Σ . In panel (c) the gap along Z_0 has been closed, yielding the homoclinic PtoP orbit Q_{Γ_2} .

This boundary value problem has a one-dimensional solution manifold, providing $B - N = n + 1 = 5$ conditions for the six free internal parameters $T^-, T^+, \varepsilon_1, \delta_1, \delta_2$ and η_0 . Figure 10(a) and (b) shows the start data for $(J_{\text{in}}, s) = (3.02661, 9.0)$, given by the orbit segments $Q_{\Gamma_1}^-$ and $Q_{\Gamma_1}^+$, the section $\Sigma = \{c_t = 38.27\}$ and the direction Z_0 . In panel (c) the gap along Z_0 has been closed via the continuation of $Q_{\Gamma_1}^-$ and $Q_{\Gamma_1}^+$, and the homoclinic PtoP orbit Q_{Γ_1} has been found as their concatenation.

A homoclinic orbit connecting Γ_2 to itself can be computed in exactly the same way, by considering $Q_{\Gamma_2}^-$ and $Q_{\Gamma_2}^+$ from Γ_2 to a section Σ near Γ_1 and back. In fact, the same initial data from the PtoP heteroclinic orbit can be used for these orbits. Specifically, we set $Q_{\Gamma_2}^- \subset \mathcal{Q}_0$ and $Q_{\Gamma_2}^+ = Q_1$, with the difference being that Σ is now chosen through the end points of $Q_{\Gamma_2}^-$ and $Q_{\Gamma_2}^+$ near Γ_1 . Figure 11(a) shows this start data for $(J_{\text{in}}, s) = (3.02661, 9.0)$, where the section is now $\Sigma = \{c_t = 33.95\}$. Panel (b) shows the direction Z_0 with an initial gap η_0 between the end points of $Q_{\Gamma_2}^-$ and $Q_{\Gamma_2}^+$ in Σ . Continuation of $Q_{\Gamma_2}^-$ and $Q_{\Gamma_2}^+$ as solutions of (6)–(10) and (19) and detection of $\eta_0 = 0$ gives the homoclinic PtoP orbit Q_{Γ_2} ; see Fig. 11(c).

In the continuation runs to close the gap η_0 to find the Q_{Γ_1} and Q_{Γ_2} the system parameters J_{in} and s remained fixed. Indeed, for every fixed value of J_{in} and s the homoclinic PtoP orbits Q_{Γ_1} and Q_{Γ_2} are each a unique solution of the BVP (6)–(10) and (19) with $\eta_0 = 0$. As such, they can be continued (together with the respective

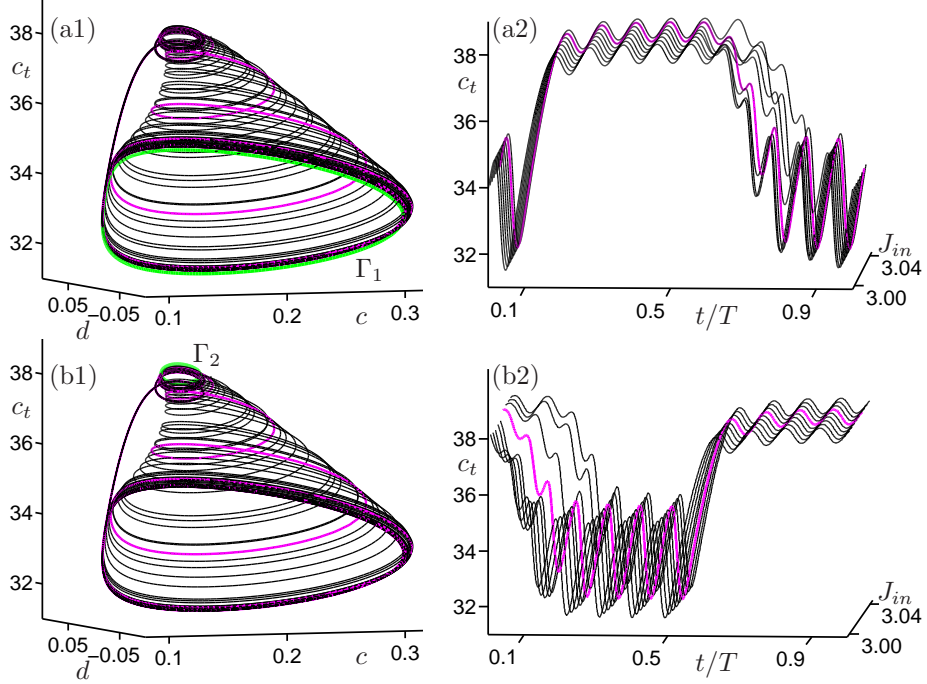


Figure 12: PtoP homoclinic orbits of Γ_1 (a1)–(a2) and of Γ_2 (b1)–(b2) continued in the system parameter J_{in} over the interval $[3.0, 3.04]$ for fixed $s = 9.0$. Panels (a1) and (b1) shows selected homoclinic orbits in projection onto (c, d, c_t) -space, and panels (a2) and (b2) show them as a waterfall diagram of time series of c_t over the unit time interval. The PtoP homoclinic orbits for $J_{\text{in}} = 3.02661$, Q_{Γ_1} from Fig. 10 and Q_{Γ_2} from Fig. 11, are highlighted.

periodic orbits and their Floquet vectors) in any system parameter. Figure 12 shows results of their continuation in J_{in} over the interval $[3.0, 3.04]$, namely, of Q_{Γ_1} in row (a) and of Q_{Γ_2} in row (b). Panels (a1) and (b1) show selected PtoP homoclinic orbits in projection onto (c, d, c_t) -space, demonstrating that they indeed are close to the PtoP heteroclinic cycle between Γ_1 and Γ_2 ; compare with Fig. 7. Notice further from Fig. 12(a1) that for any $J_{\text{in}} \in [3.0, 3.04]$ the PtoP homoclinic orbit Q_{Γ_1} closely follows the codimension-one PtoP connection Q_1 from Γ_1 to Γ_2 , while different orbits from the one-parameter family \mathcal{Q}_0 of codimension-zero PtoP connections are followed back to Γ_1 . The waterfall diagram in Fig. 12(a2) shows that, as J_{in} is increased, the number of loops of Q_{Γ_1} near the periodic orbit Γ_2 increases from about five to about six; this is consistent with the fact that the computed family Q_{Γ_1} in Fig. 12(a1) ‘covers’ the entire cylinder of the PtoP heteroclinic cycle in Fig. 7 as J_{in} increases. The corresponding statement holds for the continuation of the PtoP homoclinic orbits Q_{Γ_2} in Fig. 12(b1), where now the number of loops near the periodic orbit Γ_1

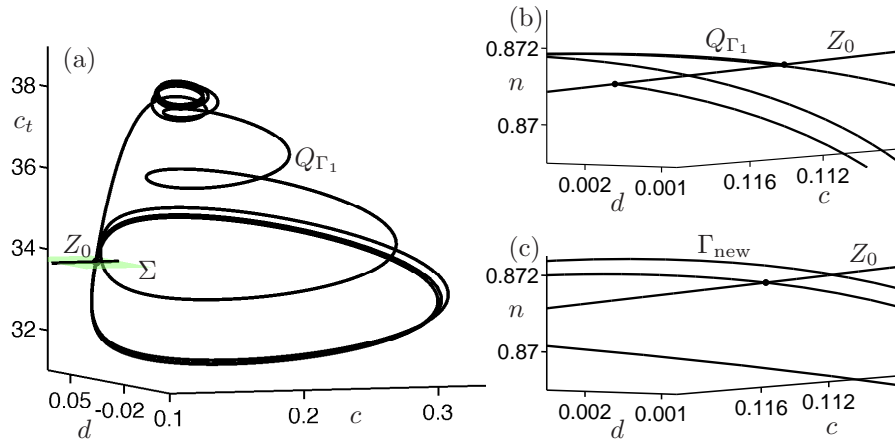


Figure 13: Finding a saddle periodic orbit by continuation from the PtoP homoclinic orbit Q_{Γ_1} for $(J_{\text{in}}, s) = (3.02661, 9.0)$ from Fig. 10. Panel (a) shows the orbit segment Q_{Γ_1} whose endpoints lie in the section $\Sigma = \{c_t = 33.95\}$, and panel (b) shows Q_{Γ_1} near the direction Z_0 in Σ . In panel (c) the gap along Z_0 has been closed by continuation in the internal parameters T^- and η_0 until $\eta_0 = 0$, yielding a saddle periodic orbit Γ_{new} .

decreases in panel (b2) from about five to about three.

We finish by showing how saddle periodic orbits near PtoP homoclinic orbits can be computed. As an example we compute a periodic orbit near Q_{Γ_1} . The idea is simply to close the gap between the two end points of Q_{Γ_1} . Therefore, we choose the section $\Sigma = \{c_t = 33.95\}$ and the direction Z_0 defined by these end points, with gap η_0 . This initial data is shown in Fig. 13(a) and (b). The orbit segment Q_{Γ_1} is a solution of the smaller BVP given by (6), (10) and (19), which provides $B - N = (n + 1) - n = 1$ condition for the two free internal parameters T^- and η_0 . Continuing solutions of this BVP until $\eta_0 = 0$ yields a saddle periodic orbit Γ_{new} that closely follows the original PtoP homoclinic orbit Q_{Γ_1} ; see Fig. 13(c). Once it has been found, Γ_{new} can be continued in system parameters, as usual, as a solution of the standard periodic orbit BVP (12)–(14).

7 Conclusions

We have presented the first example of a concrete vector field in which a non-structurally stable PtoP heteroclinic cycle connecting two saddle periodic orbits has been located numerically. Specifically, we showed that a four-dimensional model of intracellular calcium dynamics has a bifurcation structure with the necessary geometric ingredients, and then identified a codimension-one PtoP cycle numerically with an implementation of Lin’s method. The PtoP cycle was then continued as a curve in the relevant two-parameter plane of the system. We also computed two nearby homoclinic orbits of periodic orbits and a new saddle periodic orbit.

Our computations provide evidence for a considerable level of maturity in numerical techniques for the detection and continuation of global objects. In particular, the Lin’s method approach that we employed here can be used, in principle, to identify and continue in parameters any homoclinic or heteroclinic chain involving a (finite) number of equilibria and periodic orbits, as well as nearby global objects. The ability to do these kinds of computations can be very useful in the context of applications. For example, termination mechanisms for homoclinic curves in the context of models of various excitable systems were discussed in [10]. One of the mechanisms considered in [10] and investigated further in [11] is a so-called EP1t point, which is a codimension-two bifurcation that can occur at parameter values for which there is simultaneously a codimension-one heteroclinic connection from an equilibrium to a periodic orbit and a codimension-one heteroclinic tangency between the unstable manifold of the periodic orbit and the stable manifold of the equilibrium. The analysis in [11] makes predictions about the scaling of turning points of branches of homoclinic bifurcations of equilibria and of the loci of saddle-node of limit cycles bifurcations in the vicinity of an EP1t point; numerical evidence consistent with these predictions was given for several models in [11], and provided indirect evidence for the existence of EP1t points in these models. However, the EP1t points were not computed directly. Other global bifurcations such as PtoP heteroclinic bifurcations are also thought to occur near EP1t points, but, similarly, have not been directly computed because of the lack of appropriate numerical algorithms. Thus, the availability of methods such as those outlined in this paper will enable fuller investigation of models of this type, and may consequently lead to a better understanding of their dynamics.

We would argue that the availability of concrete vector field models in combination with advanced numerical tools may also be of benefit for theoretical investigations of higher-dimensional dynamical phenomena as they occur in vector fields on \mathbb{R}^n with $n \geq 4$ or, equivalently, in diffeomorphisms on \mathbb{R}^k with $k \geq 3$. A key role in this field is played by heterodimensional cycles (also referred to as cycles with unstable dimension variability) in diffeomorphisms between saddle points with different dimensions of their stable and unstable manifolds [2, 8, 9, 17, 39]. As was mentioned in Sec. 2.1, the PtoP cycle of codimension one presented in Fig. 1 constitutes the minimal example of such a heterodimensional cycle. Roughly speaking, the

recurring passage along such a cycle generates chaotic dynamics that is more complicated (in a well-defined sense) than the ‘usual’ chaos that one knows from planar diffeomorphisms and three-dimensional vector fields; see [8, 9, 17]. Hence, the study of the codimension-one PtoP cycle and its nearby dynamics in the calcium model discussed here is of interest beyond the specific application, as a way to illustrate and further motivate theoretical investigations of heterodimensional cycles.

Acknowledgements

The authors thank Enrique Pujals for helpful discussions concerning the dynamics near heterodimensional cycles.

References

- [1] P. Aguirre, E. J. Doedel, B. Krauskopf and H. M. Osinga, *Investigating the consequences of global bifurcations for two-dimensional invariant manifolds of vector fields*, *Discr. Contin. Dynam. Syst. — Series A*, **29**(4) (2011) 1309–1344.
- [2] K. T. Alligood, E. Sander and J. A. Yorke, *Crossing bifurcations and unstable dimension variability*, *Phys. Rev. Lett.*, **96**(24) (2006) 244103.
- [3] A. Atri, J. Amundsen, D. Clapham and J. Sneyd, *A single-pool model for intracellular calcium oscillations and waves in the *Xenopus laevis* oocyte*, *Biophysical Journal*, **65** (1993) 1727–1739.
- [4] W.-J. Beyn *The numerical computation of connecting orbits in dynamical systems*, *IMA J. Numer. Anal.*, **10** (1990) 379–405.
- [5] W.-J. Beyn *On well-posed problems for connecting orbits in dynamical systems*, *Cont. Math. Chaotic Numerics*, **172** (1994) 131–68.
- [6] M. P. Boer, B. W. Kooi and S. A. L. M. Kooijman, *Homoclinic and heteroclinic orbits to a cycle in a tri-trophic food chain*, *J. Math. Biology*, **39**(1) (1999) 19–38.
- [7] M. P. Boer, B. W. Kooi and S. A. L. M. Kooijman, *Multiple attractors and boundary crises in a tri-trophic food chain*, *Math. Biosciences*, **169** (2001) 109–128.
- [8] C. Bonatti and L. Díaz, *Robust heteroclinic cycles and C^1 -generic dynamics*, *J. Inst. Math. Jussieu* **7**(3) (2008) 469–525.
- [9] C. Bonatti, L. Díaz and M. Viana, “Dynamics beyond uniform hyperbolicity,” Springer-Verlag, New York/Berlin, 2005.

- [10] A. R. Champneys, V. Kirk V, E. Knobloch, B. E. Oldeman and J. Sneyd, *When Shil'nikov Meets Hopf in Excitable Systems*, SIAM J. Appl. Dynam. Syst., **6** (2007) 663–693.
- [11] A. R. Champneys, E. Knobloch, V. Kirk, B. E. Oldeman, J. D. M. Rademacher, *Unfolding a tangent equilibrium-to-periodic heteroclinic cycle*, SIAM J. App. Dyn. Sys. **8** (2009) 1261–1304.
- [12] A. R. Champneys, Yu. A. Kuznetsov and B. Sandstede, *A numerical toolbox for homoclinic bifurcation analysis*, Int. J. Bif. and Chaos, **6** (1996) 867–887.
- [13] J. W. Demmel, L. Dieci and M. J. Friedman, *Computing connecting orbits via an improved algorithm for continuing invariant subspaces*, SIAM J. Sci. Comput., **22** (2000) 81–94.
- [14] B. Deng and K. Sakamoto, *Shilnikov-Hopf bifurcations*, J. Differential Equations, **119** (1995) 1–23.
- [15] F. Dercole, *User Guide to BPCONT*, Dipartimento di Elettronica e Informazione, Politecnico di Milano, 2007; available at <ftp.elet.polimi.it/outgoing/Fabio.Dercole/bpcont/bpcont.tar.gz>.
- [16] A. Dhooge, W. Govaerts, and Yu. A. Kuznetsov, *MATCONT: A Matlab package for numerical bifurcation analysis of ODEs*, ACM TOMS, **29**(2) (2003) 141–164; available at <http://www.matcont.ugent.be/>.
- [17] L. Díaz and J. Rocha, *Partially hyperbolic and transitive dynamics generated by heteroclinic cycles*, Ergod. Th. Dynam. Sys., **21** (2001) 25–76
- [18] L. Dieci and J. Rebaza, *Point-to-periodic and periodic-to-periodic connections*, BIT Numerical Mathematics, **44** (2004) 41–62.
- [19] L. Dieci and J. Rebaza, *Erratum: Point-to-periodic and periodic-to-periodic connections*, BIT Numerical Mathematics, **44** (2004) 617–18.
- [20] E. J. Doedel, *Lecture notes on numerical analysis of nonlinear equations*, in B. Krauskopf, H. M. Osinga and J. Galán-Vioque (Editors) “Numerical Continuation Methods for Dynamical Systems,” Springer-Verlag, New York/Berlin, 2007.
- [21] E. J. Doedel, with major contributions from A. R. Champneys, T. F. Fairgrieve, Yu. A. Kuznetsov, B. E. Oldeman, R. C. Paffenroth, B. Sandstede, X. J. Wang, and C. Zhang. AUTO-07P: Continuation and bifurcation software for ordinary differential equations; available at <http://cmvl.cs.concordia.ca/>.
- [22] E. J. Doedel and M. J. Friedman, *Numerical computation of heteroclinic orbits*, J. Comput. Appl. Math., **26** (1989) 155–170.

- [23] E. J. Doedel, B. W. Kooi B W, Yu. A. Kuznetsov and G. A. K. Voorn, *Continuation of connecting orbits in 3D-ODES: I. Point-to-cycle connections*, Int. J. Bifurc. Chaos, **18** (2008) 1889–1903.
- [24] E. J. Doedel, B. W. Kooi B W, Yu. A. Kuznetsov and G. A. K. Voorn, *Continuation of connecting orbits in 3D-ODES: II. Cycle-to-cycle connections*, Int. J. Bifurc. Chaos, **19** (2008) 159–169.
- [25] E. J. Doedel, B. Krauskopf and H. M. Osinga, *Global bifurcations of the Lorenz manifold*, Nonlinearity **19**(12) (2006) 2947–2972.
- [26] J. P. England, B. Krauskopf and H. M. Osinga, *Computing one-dimensional global manifolds of Poincaré maps by continuation*, SIAM J. Appl. Dynam. Syst., **4** (2005) 1008–1041.
- [27] M. Falcke, *Reading the patterns in living cells: the physics of Ca^{2+} signaling*, Adv. Phys., **53** (2004) 255–440.
- [28] E. Freire, A.J. Rodriguez-Luis, E. Gamero and E. Ponce, *A case study for homoclinic chaos in an autonomous electronic circuit: A trip from Takens-Bogdanov to Hopf-Shilnikov*, Physica D, **62**(1-4) (1993) 230–253.
- [29] M. Friedman and E. J. Doedel, *Numerical computation and continuation of invariant manifolds connecting fixed points*, SIAM J. Numer. Anal., **28**(3) (1991), 789–808.
- [30] M. Friedman and E. J. Doedel, *Computational methods for global analysis of homoclinic and heteroclinic orbits: A case study*, J. Dyn. Diff. Eq., **5** (1993) 37–57.
- [31] J. Guckenheimer and P. Holmes, “Nonlinear Oscillations, Dynamical Systems and Bifurcations of Vector Fields,” 2nd edition, Springer-Verlag, New York/Berlin, 1986.
- [32] E. Harvey, V. Kirk, J. Sneyd and M. Wechselberger, *Multiple time-scales, mixed mode oscillations and canards in intracellular calcium models*, J. Nonlinear Science, **21**(5) (2011) 639–683.
- [33] P. Hirschberg and E. Knobloch, *Shilnikov-Hopf bifurcation*, Phys. D, **62** (1993) 202–216.
- [34] A. J. Homburg and B. Sandstede, *Homoclinic and heteroclinic bifurcations in vector fields*, in H. Broer, F. Takens and B. Hasselblatt (Editors), “Handbook of Dynamical Systems III,” Elsevier, 2010, pp. 379–524.
- [35] J. Knobloch, *Lin’s method for discrete dynamical systems*, J. Difference Equations and Applications, **6** (2000) 577–623.

- [36] J. Knobloch, “Lin’s Method for Discrete and Continuous Dynamical Systems and Applications,” Habilitationsschrift, TU Ilmenau, 2004.
- [37] J. Knobloch and T. Rieß, *Lin’s method for heteroclinic chains involving periodic orbits*, *Nonlinearity*, **23**(1) (2010) 23–54.
- [38] J. Knobloch, T. Rieß and M. Vielitz, *Nonreversible homoclinic snaking*, *Dynamical Systems*, **26**(3) (2011) 335–365.
- [39] E. J. Kostelich, I. Kan, C. Grebogi, E. Ott and J. A. Yorke, *Unstable dimension variability: A source of nonhyperbolicity in chaotic systems*, *Physica D*, **109**(1–2) (1997) 81–90.
- [40] B. Krauskopf and B. E. Oldeman, Bifurcations of global reinjection orbits near a saddle-node Hopf bifurcation *Nonlinearity* **19** (2006) 2149–67.
- [41] B. Krauskopf, H. M. Osinga and J. Galán-Vioque (Editors) “Numerical Continuation Methods for Dynamical Systems,” Springer-Verlag, New York/Berlin, 2007.
- [42] B. Krauskopf and T. Rieß, *A Lin’s method approach to finding and continuing heteroclinic orbits connections involving periodic orbits*, *Nonlinearity* **21** (2008) 1655–1690.
- [43] Yu. A. Kuznetsov, “Elements of Applied Bifurcation Theory,” 3rd edition, Springer-Verlag, New York/Berlin, 2004.
- [44] Yu. A. Kuznetsov, O. De Feo, and S. Rinaldi, *Belyakov homoclinic bifurcations in a tritrophic food-chain model*, *SIAM J. Appl. Math.*, **62** (2001) 462–487.
- [45] X.-B. Lin, *Using Melnikov’s method to solve Shilnikov’s problems*, *Proc. R. Soc. Edinb.*, **A116** (1990), 295–325.
- [46] B. E. Oldeman, A. R. Champneys, and B. Krauskopf. *Homoclinic branch switching: a numerical implementation of Lin’s method*. *Internat. J. Bifur. Chaos Appl. Sci. Engrg.*, **13**(10) (2003) 2977–2999.
- [47] J. Palis and W. de Melo. “Geometric Theory of Dynamical Systems,” Springer-Verlag, New York/Berlin, 1982.
- [48] Pampel, *Numerical approximation of connecting orbits with asymptotic rate*, *Numerische Mathematik*, **90** (2001) 309–348.
- [49] J. D. M. Rademacher, *Homoclinic orbits near heteroclinic cycles with one equilibrium and one periodic orbit*, *J. Diff. Eqns.*, **218** (2005) 390–443.
- [50] J. D. M. Rademacher, *Lyapunov-Schmidt Reduction for Unfolding Heteroclinic Networks of Equilibria and Periodic Orbits with Tangencies*, *J. Diff. Eq.*, **249** (2010) 305–348.

- [51] T. Rieß, “Using Lin’s method for an almost Shilnikov problem,” Diploma Thesis, TU Ilmenau, 2003.
- [52] B. Sandstede, “Verzweigungstheorie homokliner Verdopplungen,” PhD thesis, University of Stuttgart, 1993.
- [53] S. M. Wiczorek and B. Krauskopf *Bifurcations of n -homoclinic orbits in optically injected lasers*, Nonlinearity, **18** (2005) 1095–1120.
- [54] A. C. Yew, *Multipulses of nonlinearly-coupled Schrödinger equations*, J. Diff. Eqns., **173** (2001) 92–137.
- [55] W. Zhang, V. Kirk, J. Sneyd, M. Wechselberger, *Changes in the criticality of Hopf bifurcations due to certain model reduction techniques in systems with multiple timescales*, J. Math. Neuroscience, **1** (9) (2011).